

Accurate Small-Signal Modeling of Digitally Controlled Buck Converters with ADC-PWM Synchronization

Hang Zhou, *Member, IEEE*, Yuxin Yang, *Student Member, IEEE*, Branislav Hredzak, *Senior Member, IEEE*
John Fletcher, *Senior Member, IEEE*

Abstract—Digital control has become increasingly widespread in modern power electronic converters. When acquiring feedback signals such as the inductor current, synchronizing the analog-to-digital converter (ADC) with the digital pulse-width modulator (DPWM) is commonly employed to accurately track their steady-state average. However, the small-signal implications of such synchronization have not been investigated. This paper presents an exact small-signal model for digitally controlled buck converters operating in forced continuous-conduction mode (FCCM) under constant-frequency current-mode control, explicitly accounting for DPWM-ADC synchronization. Using a sampled-data framework, the proposed model captures all sideband effects introduced by the sampling process, yielding precise predictions of both analog and digital loop gains, even at frequencies beyond the switching and sampling frequencies. Both asymmetrical and symmetrical carrier modulations are considered. Furthermore, the digital loop gain is derived in closed form using the modified z-transform, enabling low-complexity compensator design and stability assessment. Within this framework, the analog loop gain can be directly obtained from the digital loop gain, thereby eliminating the need for computationally intensive infinite series evaluations. The validity of the proposed model is confirmed through both simulation and experimental results.

Index Terms—Digital control, sampled-data, discrete-time model, small-signal model.

I. INTRODUCTION

AS digital control becomes increasingly popular in power converters, its advantages in cost, programmability, and integration over analog designs have made it the preferred choice. [1] In particular, it greatly simplifies the realization of sophisticated algorithms. Moreover, it enables over-the-air (OTA) firmware updates, allowing deployed products to gain new functionality without hardware modifications.

In common engineering practice, digital power converter design typically begins with power stage modeling using the classical state-space averaging (SSA) technique [2], [3].

*Yuxin Yang is the corresponding author of this paper. Hang Zhou, Yuxin Yang, Branislav Hredzak and John Fletcher are with the School of Electrical Engineering & Telecommunication University of New South Wales, CO 80305 Australia (e-mail: Yuxin Yang: z5307358@ad.unsw.edu.au; Hang Zhou: hang.zhou@unsw.edu.au; Branislav Hredzak: b.hredzak@unsw.edu.au; John Edward Fletcher: (john.fletcher@unsw.edu.au)).

An analog compensator is then designed in the continuous-time domain, discretized, and finally implemented in the digital controller. By averaging the piecewise linear state-spaces over one switching period, SSA eliminates the nonlinearities. However, SSA neglects essential effects, such as computational delays, sampling, the presence of ripples, and sideband component coupling. [4] Consequently, SSA loses validity even if the perturbation frequency is far below the switching frequency. While SSA leverages well-established linear time-invariant (LTI) control theory for rapid design, it fails to provide an accurate prediction of the closed-loop stability, particularly when the crossover frequency approaches the sampling frequency, leading to a potential risk of instability.

To extend the model accuracy near or beyond the switching frequency, the sideband effect must be taken into account to form a multifrequency model [5]. As an extension to SSA, the generalized state-space averaging method (GSSA) [6]–[9] introduces Fourier series to account for higher-order harmonics in the time-domain waveforms. Based on the linear time-periodic (LTP) theory [10], the harmonic state-space (HSS) [11]–[13] and harmonic transfer function (HTF) [14], [15] methods have been proposed to model frequency coupling effects. HSS employs the harmonic balance principle [16] to represent an LTP system as an infinite-dimensional matrix equation set [5], while HTF captures both direct and cross-frequency interactions. While these multifrequency modeling methods greatly enhance accuracy, they tend to produce high-order models that are computationally intensive. Consequently, computer-based tools are required, and obtaining a simple closed-form solution is often not possible.

As a compromise between model accuracy and computational complexity, researchers have proposed simplified models that include only a limited number of sidebands. Two-frequency models proposed by [17] and [18] considered one sideband component other than the perturbed frequency f_p . By considering a pair of sideband components and the switching frequency component, [19] fixes the low-frequency phase error in two-frequency models. An extended frequency model that incorporates all sideband components to enhance accuracy under large ripple conditions was proposed in [20]. However, the analytical form of the transfer function was not provided in [20].

The describing function (DF) method [21], [22] enables accurate derivation of closed-loop transfer functions and has

been successfully applied to current-mode [23] and constant on-time (COT) [24] controlled Buck converters. It has also been extended to multiphase COT converters with phase overlapping [25], [26], and to passive-ripple architectures with exponentially decaying slopes [27]. To simplify the design process, equivalent circuit models based on Pade approximation have been proposed in [22]–[24]. Despite its impressive accuracy, the DF method provides limited physical insight, does not provide open-loop characterization, and involves cumbersome, topology-specific derivations.

Based on the sampled-data approach [28], a unified modeling method for various ripple-based control schemes is proposed in [29], [30]. By applying Shannon’s sampling theorem and infinite series summation, all sideband components are rigorously captured. Similar to the DF method, the sampled-data model remains accurate even beyond the switching frequency and does not rely on the small-ripple assumption. Additionally, it provides open-loop information and features a much simpler derivation process than DF-based models.

Although significant progress has been made in modeling analog-controlled converters, modeling efforts dedicated to digitally controlled converters remain comparatively limited. [30] extends the sampled-data approach to digitally controlled buck converters and derives an open-loop transfer function in the s -domain. Based on standard z -transform theory, [31] proposes a discrete-time model that accounts for the sampling and delay effects introduced by digital modulators, greatly simplifying digital compensator design.

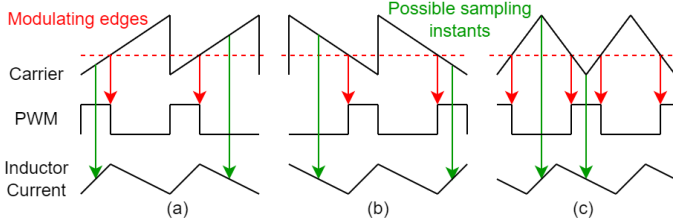


Fig. 1: PWM modulation schemes with possible synchronized ADC sampling instants (Green) and modulating edges (Red) highlighted. (a) TEM, up-counting sawtooth carrier. (b) LEM, down-counting sawtooth carrier. (c) Symmetrical modulation, triangular carrier.

The influence of modulation strategies on system dynamics has also been explored. Fig.1 presents the modulation strategies. For example, [32] studies asymmetric carrier modulations and analyzes how leading-edge modulation (LEM) and trailing-edge modulation (TEM) affect loop stability and transient response in analog modulators, while [33] further investigates symmetric carrier modulation. [34] compares LEM and TEM in digital pulse-width modulators (DPWM) and proposes a second-order global equivalent circuit to facilitate controller design. [35] demonstrates that adopting LEM in a digitally controlled boost converter can eliminate the right-half-plane zero to enhance transient performance.

In addition, [36] and [37] show that different injection points and perturbation injection methods yield different loop gain measurements in digitally controlled converters. [37] further

establishes the relationship between the responses obtained under different injection methods. Furthermore, [38] considers the case where the sampling rate is lower than the switching frequency and proposes a corresponding design methodology.

However, the impact of DPWM-ADC synchronization in digitally controlled converters has not been investigated in previous works. In practical implementations, the ADC sampling instant in digital buck converters is often dynamically aligned with the duty cycle, such that sampling occurs at the center of the on-time or off-time interval. This ensures the sampled inductor current approximates its average value under steady-state. However, such synchronization affects small-signal characteristics. The duty cycle perturbation affects the ADC samples. Despite its widespread use in engineering practice, to the authors’ best knowledge, this effect has not yet been accounted for in any existing small-signal model.

The remainder of this paper is organized as follows. Section II presents the small-signal sampled-data modeling under asymmetrical carrier modulation with explicit consideration of DPWM-ADC synchronization. A closed-form expression of the digital loop gain is derived using the modified z -transform, and it is shown that the analog loop gain can be obtained from the digital loop gain, thereby avoiding complicated infinite-series evaluations. Although the derivation begins with trailing-edge modulation (TEM), the conclusions are also extended to leading-edge modulation (LEM). Section III develops the small-signal model for the case of a symmetrical carrier. Section IV compares the proposed model with the simulation results and existing models, demonstrating its superior accuracy. Section V provides experimental validation, confirming that the proposed model exhibits good agreements in all cases. Finally, Section VI concludes the paper.

Throughout this paper, lowercase variables with a time argument (e.g. $i_L(t)$), denote time-domain signals that include both the periodic steady-state component (denoted by uppercase variables with a time argument, e.g. $I_L(t)$) and the small-signal perturbation (denoted by a hat, e.g. $\hat{i}_L(t)$). The DC value of a signal is indicated by an overline, e.g. \overline{I}_L .

II. SMALL-SIGNAL MODELING OF DIGITAL BUCK CONVERTERS WITH ASYMMETRICAL CARRIERS

Fig. 2 illustrates a digitally controlled synchronous Buck converter employing current-mode control and operating in forced continuous conduction mode (FCCM). The digital counter generates an up-counting sawtooth carrier ($CNTR$) with an amplitude of $CNTR_{MAX}$. When $CNTR$ reaches zero, the counter updates the shadow register. The shadow register serves to suppress spurious PWM pulses during abrupt changes in the duty-cycle command. The DPWM output will be high if the shadow register output is higher than $CNTR$ and will be low elsewhere. This configuration implements a TEM DPWM, in which the PWM rising edge is fixed at the beginning of each cycle, while the falling edge varies and moves according to the duty-cycle command.

To simplify the analysis, the steady-state ADC sampling instant (kT_S) defines the beginning of each cycle. The block diagram and timing are presented in Fig.2 and Fig.3, where

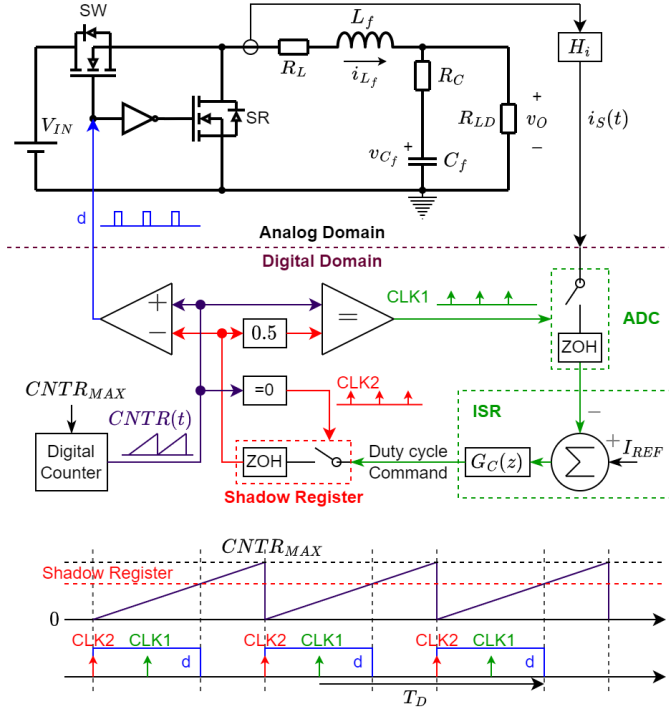


Fig. 2: A digital buck with ADC sampling at the center of the PWM On-interval and synchronized to the TEM DPWM.

H_i is the current sensor gain and T_s is the switching period. In practice, H_i also includes the ADC gain. The scaled inductor current is denoted as i_s . The duty-cycle to the inductor current transfer function and the digital PI compensator transfer function [30] are:

$$G_{id}(s) = V_{IN} \left[sL_f + R_L + \left(\frac{1}{sC_f} + R_C \right) \parallel R_{LD} \right]^{-1} \quad (1)$$

$$G_C(z) = K_P + \frac{K_i T_s}{1 - z^{-1}} \quad (2)$$

The ADC and shadow register are modeled as sample-and-hold blocks. Under the small-signal assumption, the DPWM behaves as an ideal sampler, allowing the duty-cycle perturbation \hat{d} to be treated as an impulse train [29]. When a sampling-and-hold sequence operates at the same sampling frequency, it can be equivalently represented by a single sampler followed by a delay equal to the time difference between the two sampling instants (proof provided in Appendix I). By applying this lemma twice, the 3 samplers and 2 ZOH blocks in Fig.2 can be simplified to a single sampler followed by a delay T_D , without any ZOH. Under the small-signal assumption, T_D is defined as the steady-state time between the ADC sampling instant and the moment when the new calculated duty-cycle command takes effect.

Since DPWM-ADC synchronization guarantees that sampling always occurs at the PWM on-interval center, as shown in Fig.4, in each cycle, the ADC sampling instant t_{smp} is related to the on-time perturbation \hat{t}_{on} of the previous cycle:

$$t_{smp_k} = kT_s + 0.5\hat{t}_{on}[k-1] \quad (3)$$

Under the small-signal assumption, the k -th sampled inductor current $i_L(t_{smp_k})$ can be approximated its 1st-order Taylor expansion as:

$$i_s(t_{smp_k}) \approx i_s(kT_s) + \left. \frac{di_s(t)}{dt} \right|_{t=kT_s} \times \frac{\hat{t}_{on}[k-1]}{2} \quad (4)$$

where $i_s(kT_s)$ is the scaled inductor current sampled at fixed instants kT_s , $I_s(kT_s)$ is the steady-state sampled inductor current, which equals the average inductor current \bar{I}_L :

$$i_s(kT_s) = i_s[k] = I_s(kT_s) + \hat{i}_s[k] = \bar{I}_L H_i + \hat{i}_s[k] \quad (5)$$

Extracting perturbation terms from (4) and (5) yields:

$$\hat{i}_{smp}[k] = \hat{i}_s[k] + \left. \frac{di_s(t)}{dt} \right|_{t=kT_s} \times \frac{\hat{t}_{on}[k-1]}{2} \quad (6)$$

Therefore, with (6) and Lemma 1, Fig.2 can be simplified to Fig.5. $G_{CM}(s)$ represents the analog feedback-to-modulator output transfer function and accounts for the side-band effects due to sampling, the "CM" subscript stands for controller and modulator. $G_{Plant}(z)$ denotes the plant seen by the digital PI compensator $G_C(z)$. The transfer function of the pure discrete part in Fig. 5, from $\hat{i}_s[k]$ to $\hat{t}_{on}[k]$, can be derived as:

$$G_D(z) = \frac{-G_C(z) \frac{T_s}{CNT_{R_MAX}}}{1 - [-G_C(z) \frac{T_s}{CNT_{R_MAX}}] \times H_{sync}(z)} \quad (7)$$

where the feedthrough due to DPWM-ADC alignment is:

$$H_{sync}(z) = \frac{z^{-1}}{2} \left. \frac{di_L(t)}{dt} \right|_{t=kT_s} \times H_i \quad (8)$$

According to the sampling theorem, the impulse train $\hat{i}_s[k]$'s s-domain representation $\hat{i}_s^*(s)$ is:

$$\hat{i}_s^*(s) = \hat{i}_s^*(s + jn\omega_s) = \frac{1}{T_s} \sum_{n=-\infty}^{\infty} \hat{i}_s(s + jn\omega_s) \quad (9)$$

isolating the $n = 0$ case of the infinite summation gives:

$$\hat{i}_s^*(s) = \frac{1}{T_s} \hat{i}_s(s) + \frac{1}{T_s} \sum_{\substack{n=-\infty \\ n \neq 0}}^{\infty} \hat{i}_s(s + jn\omega_s) \quad (10)$$

The second term of (10) models sideband couplings. From Fig.5, $\hat{i}_s(s)$ can be expressed as:

$$\hat{i}_s(s) = \hat{t}_{on}^*(s) e^{-sT_D} G_{id}(s) H_i \quad (11)$$

Since $\hat{t}_{on}[k]$ is also an impulse train, its s-domain representations are:

$$\hat{t}_{on}^*(s) = \hat{t}_{on}^*(s + jn\omega_s) = G_D(e^{sT_s}) \hat{i}_s^*(s) \quad (12)$$

Expanding the infinite summation term in (10) with (11) and then replacing $\hat{t}_{on}^*(s + jn\omega_s)$ with $\hat{t}_{on}^*(s)$ according to (12) gives:

$$\hat{i}_s^*(s) = \frac{1}{T_s} \left[\hat{i}_s(s) + \hat{t}_{on}^*(s) \times \sum_{\substack{n=-\infty \\ n \neq 0}}^{\infty} e^{-(s+jn\omega_s)T_D} G_{id}(s + jn\omega_s) H_i \right] \quad (13)$$

(20) agrees with the conclusion of [37] and provides a method to evaluate the analog loop gain from the digital loop gain. Furthermore, (18) resembles the modified Z-transform [39] of $G_{id}H_i$ with a sampling delay of T_D . One can perform partial fraction on $G_{id}H_i$ and then utilize the following modified Z-transform identity to evaluate (18):

$$\mathcal{Z}_m \left\{ \sum_{r=1}^{\text{PoleCount}} \frac{n_r}{s + d_r}, T_p \right\} = \sum_{r=1}^{\text{PoleCount}} \frac{n_r e^{d_r T_p}}{z e^{d_r T_s} - 1}. \quad (22)$$

where the delay T_p must satisfy $T_p \in (0, T_s)$, i.e., strictly within one sampling period. If the desired sampling delay T_D is not in this range, it can be decomposed as:

$$T_D = kT_s + T_p, \quad k \in \mathbb{Z}, T_p \in (0, T_s). \quad (23)$$

In this case, the modified z -transform of a delay T_D can be obtained by multiplying z^{-k} with the modified z -transform of a delay T_p :

$$G_{MZ}(z) = \mathcal{Z}_m\{G_{id}H_i, T_D\} = z^{-k} \mathcal{Z}_m\{G_{id}, T_p\} H_i. \quad (24)$$

where in the case of TEM, $k = 1$ and $T_p = 0.5DT_s$, as shown in Fig.2 and Fig.3.

The above analysis for TEM can be extended to LEM. Table I summarizes the effective sampling delay T_D under different modulation modes and sampling strategies.

TABLE I: T_D Under Various Asymmetrical Modulations and Different Sampling Positions

Modulation + Sampling Position	k	T_p
TEM, Sample at the on-interval center	1	$0.5DT_s$
TEM, Sample at the off-interval center	0	$0.5(1 + D)T_s$
LEM, Sample at the on-interval center	0	$(1 - 0.5D)T_s$
LEM, Sample at the off-interval center	1	$0.5(1 - D)T_s$

By applying (24) to (17), the plant transfer function seen by the digital compensator can be obtained for both TEM and LEM cases, which provides the basis for loop compensation design, e.g., using the pole-placement method.

III. SMALL-SIGNAL MODELING OF DIGITAL BUCK CONVERTERS WITH SYMMETRICAL CARRIERS

The above analysis for asymmetrical carriers can be extended to the case where the carrier is a symmetric triangular waveform. Fig.6 illustrates the key waveforms of a digital buck converter with a triangular carrier. The ADC samples when $CNTR$ reaches 0, which corresponds to the center of the PWM on-interval. Afterwards, the new duty cycle command is loaded into the shadow register when $CNTR$ reaches $CNTR_{MAX}$. Compared to the asymmetrical case, two important differences arise. First, in the symmetrical case, the ADC sampling instant is always fixed with respect to the carrier and does not vary with any perturbation. Consequently, there will be no $H_{sync}(z)$. Second, each impulse $\hat{t}_{on}[k]$ now maps to two impulses in \hat{d} that have different delays (T_{D1} and T_{D2}), which is similar to the sampled-data COT model in [30].

In this case, the plant transfer function in the z -domain seen by the digital compensator is given by:

$$G_{\text{Plant,SYM}}(z) = \frac{T_s}{2CNTR_{\text{max}}} \left(\mathcal{Z}_m\{G_{id}, T_{D1}\} + \mathcal{Z}_m\{G_{id}, T_{D2}\} \right) H_i \quad (25)$$

where T_{D1} and T_{D2} are given in Table II. This table also accounts for the alternative configuration where sampling occurs at the off-interval center, i.e., when $CNTR = CNTR_{\text{max}}$ and the shadow register is updated at $CNTR = 0$.

TABLE II: T_{D1} and T_{D2} Under Symmetrical Modulation and Different Sampling Positions

Sampling Position	T_{D1}	$T_{D2} - T_{D1}$
Sample at the on-interval center	$(1 - 0.5D)T_s$	DT_s
Sample at the off-interval center	$0.5(1 + D)T_s$	$(1 - D)T_s$

(25) provides the plant transfer function for digital compensator design. The open-loop transfer function in the digital domain can then be computed from (19), while the corresponding analog-domain loop gain can still be obtained directly using (20). In this case, $T_0(s)$ is modified as:

$$T_{0,\text{SYM}}(s) = \frac{G_c(e^{sT_s})}{2CNTR_{\text{max}}} (e^{-sT_{D1}} + e^{-sT_{D2}}) G_{id}(s) H_i \quad (26)$$

IV. COMPARISON BETWEEN EXISTING SMALL-SIGNAL MODELS AND THE PROPOSED ANALYTICAL MODEL

For a fair comparison, all models are evaluated under the same set of circuit and control parameters, summarized in Table III.

TABLE III: Parameters Used for Model Comparison

Symbol	Description	Value
V_{IN}	Input voltage	12V
D	Steady-state duty cycle	27.596%
T_s	Switching period	10 μ s
L_f	Inductance	6 μ H
R_L	DC winding resistance (DCR) of L_f	1m Ω
C_f	Output capacitance	100 μ F
R_C	Equivalent series resistance (ESR) of C_f	10m Ω
R_{LD}	Load resistance	0.33 Ω
$CNTR_{MAX}$	Digital counter upper bound	1.2
K_p	Compensator proportional gain	0.2
K_i	Compensator integration gain	31420

Fig. 7 compares the analog loop gain predicted by the proposed model, Yan's model [30], and SIMPLIS simulation. The results were obtained under TEM modulation with turn-off-centered sampling. Since the proposed model explicitly incorporates the DPWM-ADC synchronization effect through the $H_{sync}(z)$ term, its prediction shows excellent agreement with the simulation results. In contrast, Yan's model [30] deviates by more than 45 dB lower, translating to significant inaccuracies in the predicted closed-loop gain ($T_c(s) = T_i(s)/(1 + T_i(s))$ [29]), as depicted in Fig. 8. This observation further confirms that, in a digitally controlled power converter, without proper synchronization between the ADC and the DPWM, the steady-state error cannot be fully eliminated even if the digital compensator contains an integral term.

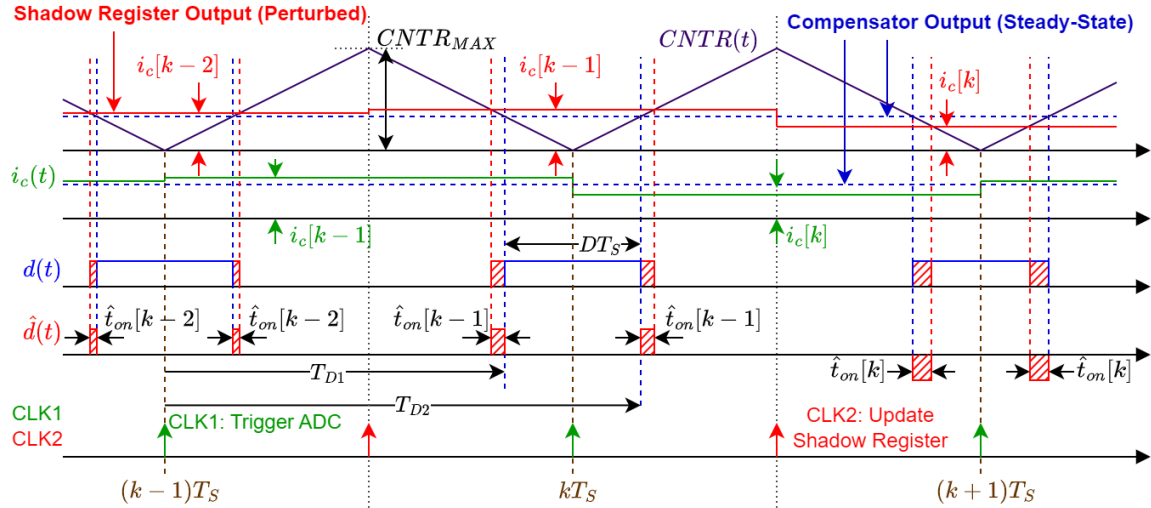


Fig. 6: Key discrete domain waveforms of a digital buck converter with a symmetrical carrier, the horizontal dashed blue line represents the steady-state duty-cycle command, the vertical dashed brown line marks the steady-state ADC sampling instant.

Fig.9 presents the plant transfer function as perceived by the digital compensator, predicted by the proposed model, Dragan’s purely discrete-time model [31], and SIMPLIS simulations. It is observed that Dragan’s model, which neglects DPWM-ADC synchronization, consistently deviates from the simulation results. In contrast, the proposed model achieves an excellent match across the entire frequency range, validating its superior accuracy.

Fig. 10 illustrates the analog and digital loop gains using different perturbation methods. As reported in [36], [37], the two measurements exhibit close agreement in the mid-frequency range (approximately 100 Hz to half the switching frequency), but significant discrepancies appear at both low and high frequencies. At low frequencies, the digital loop gain behaves as an ideal integrator, theoretically yielding an infinite DC gain, whereas the analog loop gain settles to a finite value. This property can be rigorously verified by evaluating the limits of (20) and (19) as $s \rightarrow 0$.

To further verify the effectiveness of the proposed model, Fig. 11 compares its predictions against SIMPLIS simulations under symmetrical modulation, where the ADC sampling is performed at the turn-off center.

TABLE IV: Comparison between the proposed model and existing models of digital DC-DC converters

Model	Consider DPWM-ADC Alignment	Perspective	Modulation	Complexity
Yan’s [30]	No	Analog	TEM	Moderate
Dragan’s [31]	No	Digital	TEM	Low
Lin’s [36]	No	Analog	TEM	High
This work	Yes	Analog & Digital	TEM, LEM, Symmetrical	Low

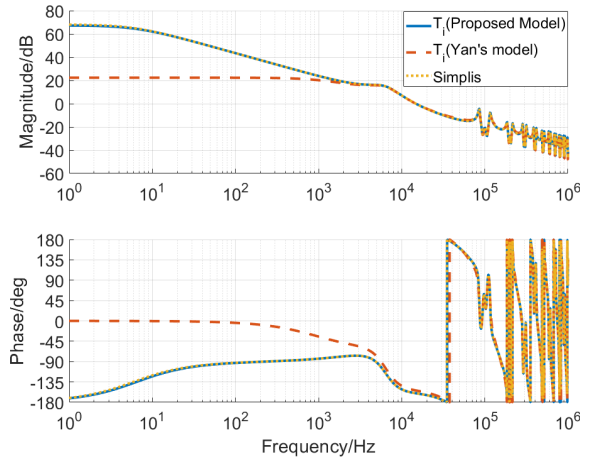


Fig. 7: Analog loop gain (TEM + turn-off-centered sampling): the proposed model, Yan’s model [30], and simulation.

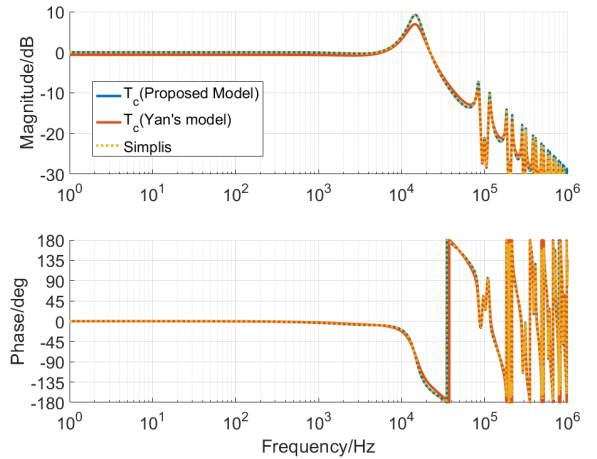


Fig. 8: Analog closed-loop transfer function (TEM + turn-off-centered sampling): the proposed model, Yan’s model [30], and simulation.

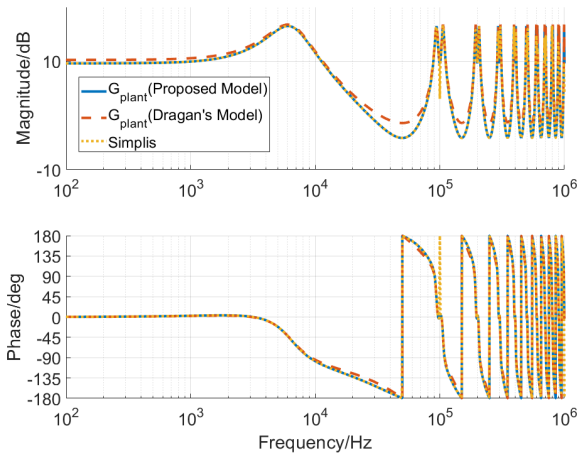


Fig. 9: Plant transfer function as perceived by the digital compensator (TEM + turn-off-centered sampling): the proposed model, Dragan's model [31], and simulation.

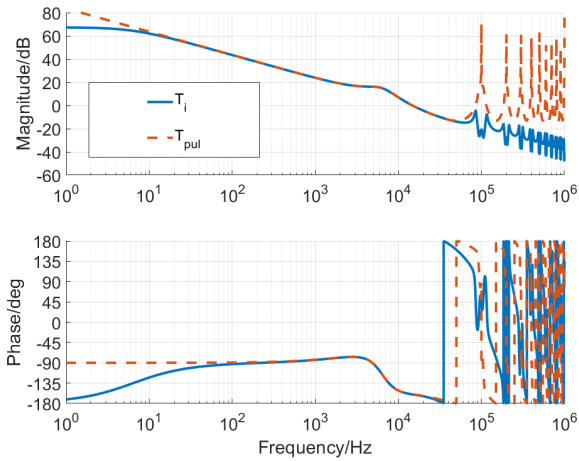


Fig. 10: Analog and digital loop gains predicted by the proposed model (TEM + turn-off-centered sampling).

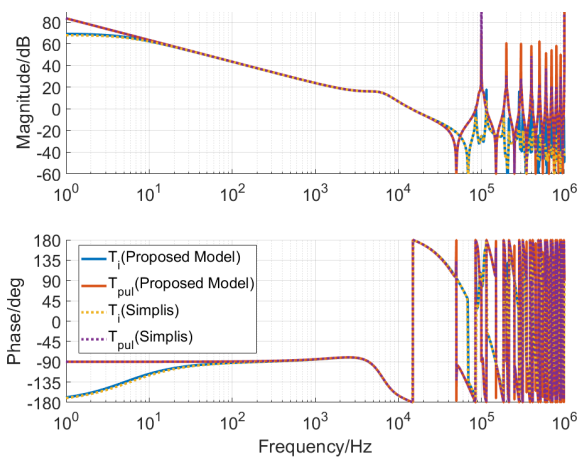


Fig. 11: Analog and digital loop gains under symmetrical triangular modulation with turn-off centered sampling: comparison of the proposed model and simulation.

V. EXPERIMENTAL VERIFICATION

To further validate the proposed model, a synchronous buck converter prototype was built as shown in Fig. 12. The controller is implemented on a floating-point DSP (TMS320F28379) running at 200 MHz. Both the switching frequency and ADC sampling rate are set to 100 kHz. A high-resolution PWM is employed such that the PWM resolution far exceeds the 12-bit ADC resolution, thus avoiding limit cycles caused by duty-cycle quantization. Because the resolutions of DPWM and ADC are sufficiently high, quantization effects are negligible in the control operation.

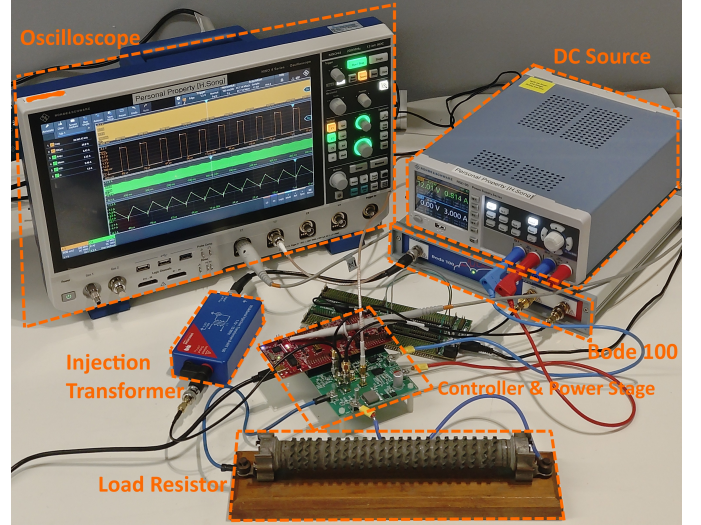


Fig. 12: Experiment setup for loop gain measurements.

To capture parasitics including the ESR and DCR, $G_{id}H_i$ is characterized by Bode 100 as:

$$G_{id}(s) \times H_i = \frac{3091003s + 5165486753}{s^2 + 12168.2939s + 648181436} \times 0.085 \quad (27)$$

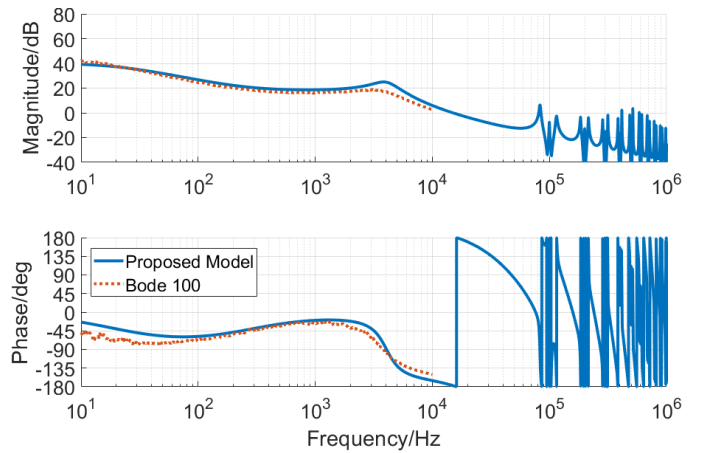


Fig. 13: Bode diagram of the calculated and measured analog loop gain.

The digital converter setup operates under TEM modulation with turn-on centered sampling, with controller gains set as $K_p = 0.2$ and $K_i = 0.2$. Fig. 13 shows the measured

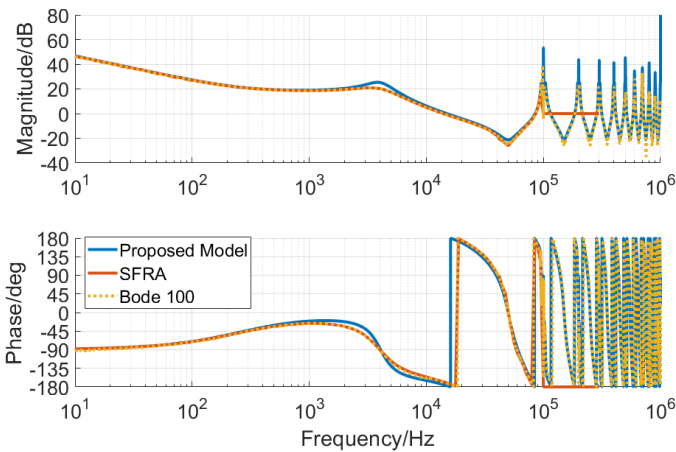


Fig. 14: Bode diagram of the calculated and measured digital loop gain.

analog loop gain. The analog loop gain is obtained via Bode 100, using an injection transformer to insert perturbations as a voltage source between the ADC input and the low-side current-sensing resistor. Two input channels of the Bode 100 measure the voltages at both ends of the injection transformer relative to ground.

Fig. 14 presents the comparison of the digital loop gain predicted by the proposed model against measurements obtained via two distinct injection methods. In the first method, akin to that in [36], the DSP samples the perturbation signal from the Bode 100 analyzer, combines it in software with the sampled inductor current, and then outputs both the pre- and post-injection current samples via DACs back to the Bode 100. The second method implements a Software-based Frequency Response Analyzer (SFRA) directly on the DSP: the SFRA injects discrete sinusoidal perturbations in software at selected frequencies and applies a Discrete-Time Fourier Transform (DTFT) to extract the magnitude and phase response at each frequency. This procedure is repeated sequentially over the frequency range to construct the bode plot. Fig. 14 demonstrates that both measurement methods yield equivalent results and closely agree with the model predictions. The discrepancy observed around 4 kHz is primarily attributed to core losses in the inductor during operation, which were not accounted for during the G_{id} characterization.

The SFRA method enables digital-loop measurement without the need for additional hardware, and when combined with the highly accurate discrete-time model proposed in this work, it provides an effective framework for digital compensator design under real operating conditions.

REFERENCES

- [1] Y. Yan, F. C. Lee, P. Mattavelli, and S. Tian, "Small-signal laplace-domain model for digital predictive current mode controls," in *2012 IEEE Energy Conversion Congress and Exposition (ECCE)*, DOI 10.1109/ECCE.2012.6342653, pp. 1386–1393, 2012.
- [2] R. Tymerski and V. Vorperian, "Generation, classification and analysis of switched-mode dc-to-dc converters by the use of converter cells," in *INTELEC '86 - International Telecommunications Energy Conference*, DOI 10.1109/INTLEC.1986.4794425, pp. 181–195, 1986.
- [3] R. D. Middlebrook and S. Cuk, "A general unified approach to modelling switching-converter power stages," in *1976 IEEE Power Electronics Specialists Conference*, DOI 10.1109/PESC.1976.7072895, pp. 18–34, 1976.
- [4] L. Harnefors, R. Finger, X. Wang, H. Bai, and F. Blaabjerg, "Vsc input-admittance modeling and analysis above the nyquist frequency for passivity-based stability assessment," *IEEE Transactions on Industrial Electronics*, vol. 64, DOI 10.1109/TIE.2017.2677353, no. 8, pp. 6362–6370, 2017.
- [5] X. Yue, X. Wang, and F. Blaabjerg, "Review of small-signal modeling methods including frequency-coupling dynamics of power converters," *IEEE Transactions on Power Electronics*, vol. 34, DOI 10.1109/TPEL.2018.2848980, no. 4, pp. 3313–3328, 2019.
- [6] S. Sanders, J. Noworolski, X. Liu, and G. Verghese, "Generalized averaging method for power conversion circuits," *IEEE Transactions on Power Electronics*, vol. 6, DOI 10.1109/63.76811, no. 2, pp. 251–259, 1991.
- [7] V. Caliskan, G. Verghese, and A. Stankovic, "Multi-frequency averaging of dc/dc converters," in *5th IEEE Workshop on Computers in Power Electronics*, DOI 10.1109/CIPE.1996.612345, pp. 113–119, 1996.
- [8] B. Lehman and R. Bass, "Extensions of averaging theory for power electronic systems," *IEEE Transactions on Power Electronics*, vol. 11, DOI 10.1109/63.506119, no. 4, pp. 542–553, 1996.
- [9] H. Li, K. Wang, J. Fang, W. Chen, and X. Yang, "High-order generalized averaging method for power electronics modeling from dc to above half the switching frequency," *IEEE Transactions on Power Electronics*, vol. 40, DOI 10.1109/TPEL.2024.3450712, no. 1, pp. 176–194, 2025.
- [10] N. M. Wereley, "Analysis and control of linear periodically time varying systems," Ph.D. dissertation, Massachusetts Institute of Technology, Cambridge, MA, USA, 1991.
- [11] G. N. Love and A. R. Wood, "Harmonic state space model of power electronics," in *2008 13th International Conference on Harmonics and Quality of Power*, DOI 10.1109/ICHQP.2008.4668792, pp. 1–6, 2008.
- [12] G. N. Love and A. R. Wood, "Harmonic state space model of power electronics," in *2008 13th International Conference on Harmonics and Quality of Power*, DOI 10.1109/ICHQP.2008.4668792, pp. 1–6, 2008.
- [13] J. Lyu, X. Zhang, X. Cai, and M. Molinas, "Harmonic state-space based small-signal impedance modeling of a modular multilevel converter with consideration of internal harmonic dynamics," *IEEE Transactions on Power Electronics*, vol. 34, DOI 10.1109/TPEL.2018.2842682, no. 3, pp. 2134–2148, 2019.
- [14] E. Mollerstedt and B. Bernhardsson, "A harmonic transfer function model for a diode converter train," in *2000 IEEE Power Engineering Society Winter Meeting. Conference Proceedings (Cat. No.00CH37077)*, vol. 2, DOI 10.1109/PESW.2000.850062, pp. 957–962 vol.2, 2000.
- [15] C. Zhang, M. Molinas, A. Rygg, J. Lyu, and X. Cai, "Harmonic transfer-function-based impedance modeling of a three-phase vsc for asymmetric ac grid stability analysis," *IEEE Transactions on Power Electronics*, vol. 34, DOI 10.1109/TPEL.2019.2909576, no. 12, pp. 12 552–12 566, 2019.
- [16] S. Ghosh, D. Das, B. Singh, S. Janardhanan, and S. Mishra, "Frequency-domain modeling of dual-active-bridge converter based on harmonic balance approach," *IEEE Journal of Emerging and Selected Topics in Industrial Electronics*, vol. 3, DOI 10.1109/JESTIE.2021.3051591, no. 1, pp. 166–176, 2022.
- [17] Y. Qiu, M. Xu, J. Sun, and F. C. Lee, "A generic high-frequency model for the nonlinearities in buck converters," *IEEE Transactions on Power Electronics*, vol. 22, DOI 10.1109/TPEL.2007.904217, no. 5, pp. 1970–1977, 2007.
- [18] Y. Qiu, M. Xu, K. Yao, J. Sun, and F. Lee, "The multi-frequency small-signal model for buck and multiphase interleaving buck converters," in *Twentieth Annual IEEE Applied Power Electronics Conference and Exposition, 2005. APEC 2005.*, vol. 1, DOI 10.1109/APEC.2005.1452961, pp. 392–398 Vol. 1, 2005.
- [19] S.-F. Hsiao, D. Chen, C.-J. Chen, and H.-S. Nien, "A new multiple-frequency small-signal model for high-bandwidth computer v-core regulator applications," *IEEE Transactions on Power Electronics*, vol. 31, DOI 10.1109/TPEL.2015.2400637, no. 1, pp. 733–742, 2016.
- [20] X. Li, X. Ruan, Q. Jin, M. Sha, and C. K. Tse, "Small-signal models with extended frequency range for dc-dc converters with large modulation ripple amplitude," *IEEE Transactions on Power Electronics*, vol. 33, DOI 10.1109/TPEL.2017.2773641, no. 9, pp. 8151–8163, 2018.
- [21] J. Li, "Current-mode control: Modeling and its digital application," Ph.D. dissertation, Virginia Polytechnic Institute and State University, Blacksburg, Virginia, USA, Apr. 2009.
- [22] J. Li and F. C. Lee, "New modeling approach and equivalent circuit representation for current-mode control," *IEEE Transactions on Power*

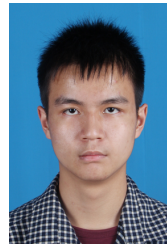
- Electronics*, vol. 25, DOI 10.1109/TPEL.2010.2040123, no. 5, pp. 1218–1230, 2010.
- [23] Y. Yan, F. C. Lee, and P. Mattavelli, “Unified three-terminal switch model for current mode controls,” *IEEE Transactions on Power Electronics*, vol. 27, DOI 10.1109/TPEL.2012.2188841, no. 9, pp. 4060–4070, 2012.
- [24] S. Tian, F. C. Lee, Q. Li, and Y. Yan, “Unified equivalent circuit model of v2 control,” in *2014 IEEE Applied Power Electronics Conference and Exposition - APEC 2014*, DOI 10.1109/APEC.2014.6803432, pp. 1016–1023, 2014.
- [25] S. Sridhar and Q. Li, “Multiphase constant on-time control with phase overlapping-part i: Small-signal model,” *IEEE Transactions on Power Electronics*, vol. 39, DOI 10.1109/TPEL.2024.3368343, no. 6, pp. 6703–6720, 2024.
- [26] S. Sridhar and Q. Li, “Multiphase constant on-time control with phase overlapping-part ii: Stability analysis,” *IEEE Transactions on Power Electronics*, vol. 39, DOI 10.1109/TPEL.2023.3345275, no. 3, pp. 3156–3174, 2024.
- [27] Y.-R. Huang and C.-J. Chen, “A novel describing function small-signal modeling approach for passive ripple constant on-time controlled converter with exponentially varying slope,” *IEEE Transactions on Power Electronics*, vol. 39, DOI 10.1109/TPEL.2024.3383855, no. 7, pp. 8425–8435, 2024.
- [28] A. R. Brown and R. Middlebrook, “Sampled-data modeling of switching regulators,” in *1981 IEEE Power Electronics Specialists Conference*, DOI 10.1109/PESC.1981.7083659, pp. 349–369, 1981.
- [29] N. Yan, X. Ruan, and X. Li, “A general approach to sampled-data modeling for ripple-based control-part i: Peak/valley current mode and peak/valley voltage mode,” *IEEE Transactions on Power Electronics*, vol. 37, DOI 10.1109/TPEL.2021.3132619, no. 6, pp. 6371–6384, 2022.
- [30] N. Yan, X. Ruan, and X. Li, “A general approach to sampled-data modeling for ripple-based control-part ii: Constant on-time and constant off-time control,” *IEEE Transactions on Power Electronics*, vol. 37, DOI 10.1109/TPEL.2021.3132624, no. 6, pp. 6385–6396, 2022.
- [31] D. Maksimovic and R. Zane, “Small-signal discrete-time modeling of digitally controlled pwm converters,” *IEEE Transactions on Power Electronics*, vol. 22, DOI 10.1109/TPEL.2007.909776, no. 6, pp. 2552–2556, 2007.
- [32] X. Li, X. Ruan, Q. Jin, M. Sha, and C. K. Tse, “Approximate discrete-time modeling of dc-dc converters with consideration of the effects of pulse width modulation,” *IEEE Transactions on Power Electronics*, vol. 33, DOI 10.1109/TPEL.2017.2752419, no. 8, pp. 7071–7082, 2018.
- [33] Y. Jiang, Y. Sun, J. Lin, S. Xie, M. Su, and Y. Liu, “Unified extended-frequency model of buck converters under different carriers,” *IEEE Transactions on Industrial Electronics*, vol. 70, DOI 10.1109/TIE.2022.3179561, no. 4, pp. 4108–4119, 2023.
- [34] Z. Li, L. Hang, Y. He, Z. He, A. Tong, D. Liu, and P. Zeng, “Sampled-data modeling and stability analysis of digitally controlled buck converter with trailing-edge and leading-edge modulations,” *IEEE Transactions on Power Electronics*, vol. 38, DOI 10.1109/TPEL.2022.3192412, no. 1, pp. 177–194, 2023.
- [35] O. Balapanuru, M. M. Lokhande, and M. V. Aware, “Performance improvement by sampling position approach in dual loop digital acm controlled dc-dc boost converter,” *IEEE Transactions on Circuits and Systems II: Express Briefs*, vol. 70, DOI 10.1109/TCSII.2022.3226562, no. 4, pp. 1565–1569, 2023.
- [36] J. Lin, M. Su, Y. Sun, X. Li, S. Xie, G. Zhang, F. Blaabjerg, and J. Feng, “Accurate loop gain modeling of digitally controlled buck converters,” *IEEE Transactions on Industrial Electronics*, vol. 69, DOI 10.1109/TIE.2021.3050389, no. 1, pp. 725–739, 2022.
- [37] X. Ruan, C. Xiong, X. Li, X. Xiong, Q. Jin, M. Sha, and C. K. Tse, “Reconsideration of loop gain and its measurement in dc-dc converters,” *IEEE Transactions on Power Electronics*, vol. 34, DOI 10.1109/TPEL.2018.2873074, no. 7, pp. 6906–6921, 2019.
- [38] P. F. Miaja, M. A. Granda, C. Fernandez, M. R. Rogina, and P. Zumel, “Discrete-time modeling of pulsewidth modulated dc-dc converters in subsampling conditions,” *IEEE Journal of Emerging and Selected Topics in Power Electronics*, vol. 9, DOI 10.1109/JESTPE.2021.3071526, no. 5, pp. 5962–5974, 2021.
- [39] E. I. Jury, *Theory and Application of the Z-Transform Method*. New York: Wiley-Interscience, 1964.



factor correction, and high-voltage power sources.

Hang Zhou (Member, IEEE) received the bachelor's and Ph.D. degrees in electrical engineering from the University of New South Wales, Sydney, NSW, Australia, in 2017 and 2022, respectively.

He is currently a Research Associate with the University of New South Wales in the field of power electronics, specializing in dc-dc converters. His research interests include low-voltage high-current dc-dc topologies, small-signal modeling of dc-dc converters, three-phase power



factor correction, and high-voltage power sources.

Yuxin Yang (Member, IEEE) was born in China. He received the Bachelor's degree in electrical engineering from the University of New South Wales (UNSW), Sydney, Australia, in 2024. He is currently pursuing the Master by Philosophy degree in electrical engineering at UNSW. His major field of research is power electronics and control systems.

He is currently conducting research on small-signal modeling of power electronic systems, sampled-data control theory, and the foundational theory of control systems. His current research focuses on unifying sampled-data models with continuous-time system representations using rigorous mathematical tools.



include the control of distributed renewable energy sources, hybrid and reconfigurable energy storage technologies, virtual power plants, and advanced control systems for power converters and energy storage systems.

Branislav Hredzak (Senior Member, IEEE) received the Ing. degree in electrical engineering from the Technical University of Kosice, Kosice, Slovak Republic, in 1993, and the Ph.D. degree in electrical engineering from the Napier University of Edinburgh, Edinburgh, U.K., in 1997. He was a Lecturer and a senior Researcher in Singapore from 1997 to 2007. He is currently an Associate Professor with the School of Electrical Engineering and Telecommunications, UNSW, Sydney, NSW, Australia. His research interests

include the control of distributed renewable energy sources, hybrid and reconfigurable energy storage technologies, virtual power plants, and advanced control systems for power converters and energy storage systems.



John Edward Fletcher (Senior Member, IEEE) received the B.Eng. (first-class Hons.) and Ph.D. degrees in electrical and electronic engineering from Heriot-Watt University, Edinburgh, U.K., in 1991 and 1995, respectively. He is currently a Professor with the University of New South Wales, Sydney, NSW, Australia. His research interests include power electronics, drives, and energy conversion. Dr. Fletcher is a Chartered Engineer in the U.K., and Fellow of the Institution of Engineering and Technology.